Atomic structure determination of the 3*C*-SiC(001) $c(4\times2)$ surface reconstruction: Experiment and theory

A. Tejeda,[1,2,*] E. Wimmer,[3] P. Soukiassian,[2,4] D. Dunham,[4,5] E. Rotenberg,[6] J. D. Denlinger,[6] and E. G. Michel[1,2]
[1]*Departamento de Física de la Materia Condensada and Instituto Nicolás Cabrera, Universidad Autónoma de Madrid, 28049 Madrid, Spain*
[2]*Commissariat à l'Energie Atomique, Laboratoire SIMA, DSM-DRECAM-SPCSI, Bâtiment 462, Saclay, 91191 Gif-sur-Yvette Cedex, France and Département de Physique, Université de Paris-Sud, 91405 Orsay Cedex, France*
[3]*Materials Design, Inc., Angel Fire, New Mexico 87710, USA and Materials Design, Inc., 72000 Le Mans, France*
[4]*Department of Physics, Northern Illinois University, DeKalb, Illinois 60115-2854, USA*
[5]*Department of Physics, University of Wisconsin—Eau Claire, Wisconsin 54702, USA*
[6]*Advanced Light Source, Lawrence Berkeley National Laboratory, Berkeley, California 94720, USA*
(Received 26 October 2006; revised manuscript received 2 March 2007; published 11 May 2007)

The structure of the Si-terminated 3*C*-SiC(001)-$c(4\times2)$ surface reconstruction is determined using synchrotron-radiation-based x-ray photoelectron diffraction from the Si 2*p* and C 1*s* core levels. Only the alternating up-and-down dimer (AUDD) model reproduces satisfactorily the experimental results. The refinement of the AUDD model leads to a height difference of (0.4±0.1) Å between the up and down Si-Si dimers. Also, the top and bottom dimers have alternating bond lengths at (2.5±0.2) Å and (2.2±0.2) Å, respectively. These results are in excellent agreement with *ab initio* density-functional calculations, which also further support the high sensitivity of this reconstruction on lateral strain and on the presence of defects. Finally, beyond well-established synchrotron-radiation-based core-level photoemission spectroscopy, an assignment is made on the structural origin of each Si 2*p* surface and subsurface shifted component, based on their different photoelectron diffraction patterns.

DOI: 10.1103/PhysRevB.75.195315 PACS number(s): 68.35.Bs, 61.14.Qp

I. INTRODUCTION

Silicon carbide (SiC) is an advanced semiconducting material with many interesting existing and potential applications.[1] Currently, it is used as structural material (e.g., in matrix composites) and in high-temperature, high-voltage, high-power, and high-frequency electronic devices and sensors.[1–5] Furthermore, it is resistant to radiation damages and rather inert chemically, making this material especially suitable for electronics working in harsh environments.[1–5] Emerging applications include catalysis, sensors, and, due to its biocompatibility, also bioengineering.[5,6] In addition, it is also a promising material for developing nanotechnologies with self-organized nano-objects or nanostructures with unprecedented characteristics[7–11] and an amazing nanochemistry.[12–16] In fact, SiC exhibits exceptional properties with average figures of merit scaling well above those of Si and III-V semiconductors (by up to 3 orders of magnitude).[5,17]

SiC is a IV-IV compound wide-band-gap semiconductor existing in more than 170 polytypes including hexagonal, cubic, and rhombohedral phases. The most used and studied polytypes are the 4H, 6H (hexagonal), and 3C (cubic) with band gaps of 3.3, 2.9, and 2.4 eV, respectively.[5] One of the important issues is the knowledge and understanding of surface atomic structure and properties. The devices often rely on the determination and control of surface layers. Among all polytypes, the surface of cubic 3*C*-SiC is of special interest because of its unusual properties. This surface was initially expected to have a behavior close to that of elemental group-IV semiconductors (Si, Ge) and due to its polar character, also of compound III-V semiconductors surfaces. However, compared to corresponding (001) faces of Si or Ge, the 3*C*-SiC(001) exhibits a much larger variety of surface reconstructions depending on Si vs C stoichiometry.[17,18] Those include the Si-terminated surfaces with (3×2) (Si-rich), $(8\times2),(5\times2),(7\times2),\ldots[(2n+1)\times2]$ (Si atomic lines) and $c(4\times2)/(2\times1)$ reconstructions, and C-terminated surfaces with $c(2\times2)$ (*sp* like), (2×1) (sp^3), and graphitic (1×1) reconstructions.[17,18] Among those, the $c(4\times2)$ and/or (2×1) reconstructions are of special interest since they are the closest to the corresponding Si(001) or Ge(001) $c(4\times2)$ and (2×1) reconstructions.[17–22] Indeed, the (2×1) reconstruction was initially proposed on the basis of low-energy electron-diffraction (LEED) and medium-energy ion scattering (MEIS) experiments, and further *ab initio* theoretical calculations for the 3*C*-SiC(001) with a Si-terminated surface on top of the first carbon plane.[23,24] Another Si-terminated surface was found later with a $c(4\times2)$ symmetry.[23–25] However, real-space scanning tunneling microscopy experiments have shown that the Si-terminated 3*C*-SiC(001) surface exhibits a $c(4\times2)$ ordering at room temperature, unlike Si(001) and Ge(001) which have a 2×1 symmetry in the same conditions.[17,26] Indeed, the (2×1) reconstruction of the 3*C*-SiC(001) surface has been shown to result from defects[26] and/or contamination of the $c(4\times2)$ surface.[27] In addition to early calculations, which also predicted a (2×1) reconstruction,[28] such a feature is at the origin of the confusion about the symmetry of this model surface. Also, an interesting temperature-induced reversible semiconducting $c(4\times2)$ to metallic (2×1) phase transition has been observed at 400 °C.[29]

Initially, the first atomic structural model for the $c(4\times2)$ reconstruction, proposed on the ground of LEED experiments, was thought to be the same as for the low-temperature Si(001) or Ge(001) surfaces, with rows of buckled Si (Ge) dimers in an anticorrelated asymmetric dimer (AAD) model having a $c(4\times2)$ symmetry.[23] Then, real-space scanning tunneling microscopy (STM) experiments, analyzing the tunneling into the filled and empty electronic states, have shown that the $c(4\times2)$ reconstruction is a Si-terminated surface, with rows of alternating up-and-down dimers (AUDDs).[26,30] This suggests a strain-driven $c(4\times2)$ surface reconstruction.[26,30] Such an AUDD model is further supported by STM image simulations using various methods,[26,31] by electronic structure photoemission (PES) measurements and calculations,[32] synchrotron-radiation-based Si $2p$ core-level photoelectron spectroscopy,[33] and by *ab initio* calculations on clusters and slabs using total-energy minimization and molecular dynamics.[31,34] In these calculations, strain was found to be important in having such an AUDD array for the $c(4\times2)$ atomic structure.[31] Subsequently, another model, the so-called missing row asymmetric dimer model (MRAD), has been proposed by *ab initio* total-energy pseudopotential calculations.[35,36] In such a model, the $c(4\times2)$ reconstruction is proposed to involve two Si adlayers (1 ML+0.5 ML).[35,36] However, such 1.5 ML Si coverage is so far not supported by experiments, neither by MEIS and reflection high-energy electron diffraction, indicating a 1 ML Si-terminated $3C$-SiC(001) $c(4\times2)$ surface,[24] by photoemission experiments,[32] nor by filled and empty state STM experiments.[26,30] Figure 1 displays schematics of the AAD, AUDD, and MRAD models.

STM provides a real-space image of the topmost surface layer at the atomic scale, giving the key central ingredients of a structural model. Indeed, STM has played a central role in solving the atomic structure of prototypical surfaces such as, e.g., the Si(111) (7×7),[37,38] and for the silicon carbide $3C$-SiC(001) (3×2) surface reconstructions,[39] providing the atomic ordering of the first surface layer. However, since it measures electronic distributions, it cannot really provide interatomic distances or atomic positions into the subsurface region. So far, STM has provided the only structural information at the atomic level for the $c(4\times2)$ reconstruction, since previous diffraction measurements were based on kinematical and not dynamical LEED,[23,25] unlike investigations performed for other $3C$-SiC(001) surface reconstructions.[40–45] The atomic structures of Si-rich (3×2) and C-terminated $c(2\times2)$ have been accurately determined using diffraction and absorption techniques, such as synchrotron-radiation-based grazing incidence x-ray diffraction, photoelectron diffraction (PED), or near-edge x-ray-absorption fine structure techniques.[41–45] So far, there are no such experimental investigations for the $c(4\times2)$ reconstruction, not even by dynamical LEED. Thus, a complete atomic structure determination, which is of central importance in addressing and understanding relevant issues such as adsorbate-surface interactions, nano-object self-formation,[7–10] and mechanisms involved in surface nanochemistry[12–16] is still lacking. Photoelectron diffraction using synchrotron radiation in the multiple-scattering mode is a state-of-the-art tool, able to probe the atomic structure of surfaces and subsurfaces. It exhibits such interesting features as chemical sensitivity and the possibility of changing the photoelectron escape depth by tuning the photon energy.[42,46–49]

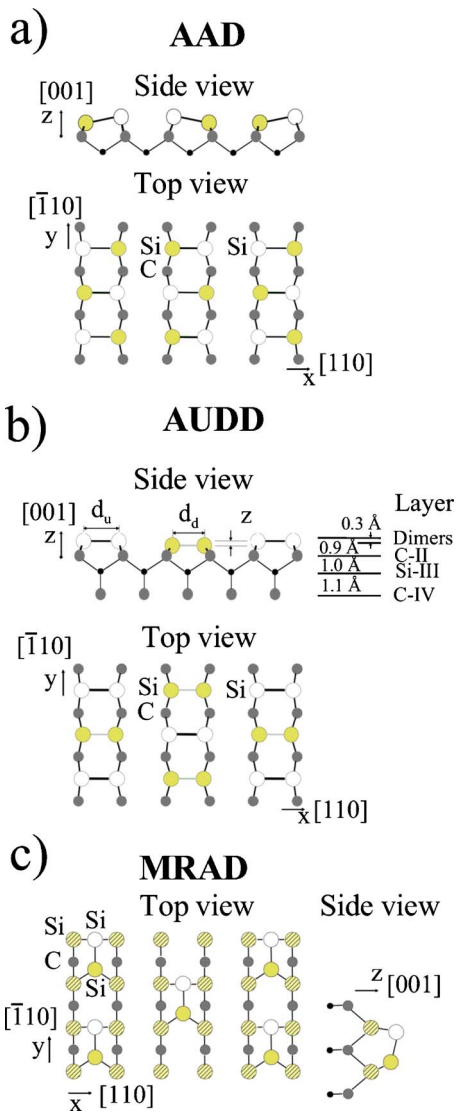

FIG. 1. (Color online) Schematic representation of the AAD, AUDD, and MRAD models, including a top view of the $c(4\times2)$ unit cell with atoms in the resulting optimized model and a side view of the model. Dark gray circles are C atoms from the second layer. AAD: white and yellow (light gray) circles correspond to up and down atoms. AUDD: white and yellow (light gray) circles are up (long) and down (short) dimers, respectively. MRAD: yellow (patterned) circles are Si atoms, while white and orange (light gray) circles are asymmetric dimers (up and down atom, respectively).

In this paper, we present a comprehensive structural experimental investigation of the $3C$-SiC(001) $c(4\times2)$ surface reconstruction. The atomic structure is determined using synchrotron-radiation-based PED in the multiple-scattering mode. The experimental work is combined with *ab initio* total-energy calculations on slab models including effects of strain and defects. In the first step, we use the PED integrated spectra to discriminate between different models. Then, we further analyze the Si $2p$ spectra with energy resolution in

order to get insights about atomic origin of the various surface and subsurface components. We use photoelectron emission from the Si $2p$ and C $1s$ core levels at different photon energies (from 150 to 340 eV) and we determine atomic positions, bond lengths, and interlayer spacing. The results indicate an atomic structure inconsistent with the AAD and the MRAD models and support the AUDD surface array of the 3*C*-SiC(001) $c(4\times2)$ reconstruction. The experimental results and the theoretical calculations are in excellent agreement, with Si dimers having alternating heights with a difference of $\Delta z=(0.4\pm0.1)$ Å (experiment) and $\Delta z=0.25$ Å (theory), and alternating lengths for the long dimer of (2.5 ± 0.2) Å (experiment) and 2.63 Å (theory) and for the short dimer of (2.2 ± 0.2) Å (experiment) and 2.36 Å (theory). The reconstruction is found to primarily affect the three topmost surface atomic layers.

II. EXPERIMENTAL DETAILS

The synchrotron-radiation-based PED experiments are performed in an ultrahigh-vacuum chamber equipped with an angle-resolving hemispherical analyzer at the 7.0.1 spherical grating monochromator beam line, using the light emitted by the Advanced Light Source (ALS, Berkeley) third generation storage ring. The pressure during the experiment is 1×10^{-10} Torr. We use single-crystal, single-domain 3*C*-SiC(001) thin films (≈1 μm) grown by chemical-vapor deposition on a 4° off vicinal Si(001) surface at CEA-LETI, Grenoble. High quality $c(4\times2)$ surface reconstructions were prepared and checked before and after each data set to be free from contamination by photoemission spectroscopy and to exhibit a sharp $c(4\times2)$ LEED pattern. The measurements were made using a Phi OMNI-IV electron energy analyzer. Both polar and azimuthal angles are varied by sample rotation. The sample is oriented by LEED and by angle-resolved photoelectron diffraction scans. The sample symmetry is previously checked with several 180° azimuthal cuts. The [110] direction is taken as the reference for azimuthal emission angles (i.e., at $\phi=0$), and for polar emission angles along the [001] direction (normal emission, i.e., $\theta=0$). A series of azimuthal scans (ϕ, azimuthal emission angle) is obtained by rotating the sample around its normal in a 100° and 120° ϕ-range for Si $2p$ and C $1s$ photoemitted electrons, respectively. The polar emission angle θ is varied between 0° and 72° (8° steps for Si $2p$ emission and 4.5° steps for C$1s$ emission). Si $2p$ (C $1s$) intensity is recorded at 150, 175, and 210 eV (340 eV). The absolute angular precision is 1° for both θ and ϕ. The number of sampled points for the Si $2p$ (C $1s$) emission is 105 (320). The total-energy resolution (analyzer+monochromator) is 60 meV at Si $2p$ and <100 meV at C $1s$. All other details about high quality SiC surface preparation procedures are described elsewhere.[17,26,30,32,33]

III. COMPUTATIONAL DETAILS

A. Photoelectron diffraction simulations

In a photoemission experiment, the outgoing electron wave field is diffracted by the atoms in the vicinity of the emitter. This phenomenon is used in the PED technique to obtain structural information. A spherical-wave multiple-scattering cluster formalism[50] up to the 11th order of scattering is used to reproduce the data and discern the correct surface structure of 3*C*-SiC(001)-$c(4\times2)$. We use a cluster of more than 2700 atoms, with a mean-free-path dependent attenuation of the electron yield, considered as an adjustable parameter within the order of magnitude given by Ref. 51. Simulated PED patterns are generated by EDAC code with emitters at symmetry-inequivalent sites in the first to seventh topmost interface layers.[50] We consider the AAD model,[23] the MRAD model,[35,36] the AUDD model,[26,30] and what we have named as AUDD-Si model, which consists of a Si-terminated 3*C*-SiC(001) surface below the Si symmetric dimers in a similar configuration as in AUDD. In MRAD or AAD models, we simulate two-domain samples, corresponding to 180° rotation. The Si and C muffin-tin scattering phase shifts are used. The quality of the surface model is judged on the basis of the agreement between theory and experiment, as measured by the figure of merit R (R_1 factor of Saiki *et al.*[52] and Van Hove *et al.*[53]). The surface model is modified until a good value of R is reached, as also confirmed by visual inspection.

The atomic structure of the models is refined from the low kinetic energy data analysis. To this end, Si $2p$ spectra are integrated to obtain the experimental anisotropy curves, which are compared to the simulation. The atomic positions are varied during the refinement process, preserving the mirror plane along the [110] ($[\bar{1}10]$) direction in the AUDD (MRAD) model. In the MRAD model, the vertical coordinates of all the atoms in the outermost Si layers are varied, as well as the coordinates parallel to the $[\bar{1}10]$ direction. In the AUDD model, the vertical coordinates of the last three layers and the bond lengths of the dimers are varied. Dimers are also allowed to become asymmetric. Thus, all the surface structural parameters of the clusters are modified until an absolute minimum in R factor is found.

B. *Ab initio* computations

The atomic structure of the $c(4\times2)$ reconstruction has also been studied by computations based on the density-functional theory[54] with the generalized gradient approximation[55] and all-electron frozen-core projector-augmented-wave potentials[56] as implemented in the Vienna *ab initio* simulation package[57] (VASP) within the MedeA software environment.[58] The SiC(001) surface is represented by a repeated slab model. Each slab consists of a $c(4\times2)$ supercell of 11 atomic layers, terminated above and below by silicon atoms. The vacuum distance between the slabs is approximately 10 Å, which is sufficient to avoid spurious interactions between the slabs.

Seven different sets of lattice parameters parallel to the surface are chosen, which correspond to lateral strains between −1% and +5% in both the x and y directions. These strains are defined with respect to the computed equilibrium bulk SiC lattice parameter. In the calculations of the surface reconstruction, an initial bias is introduced by slightly lifting the central dimer. Then, all atomic positions in the model are

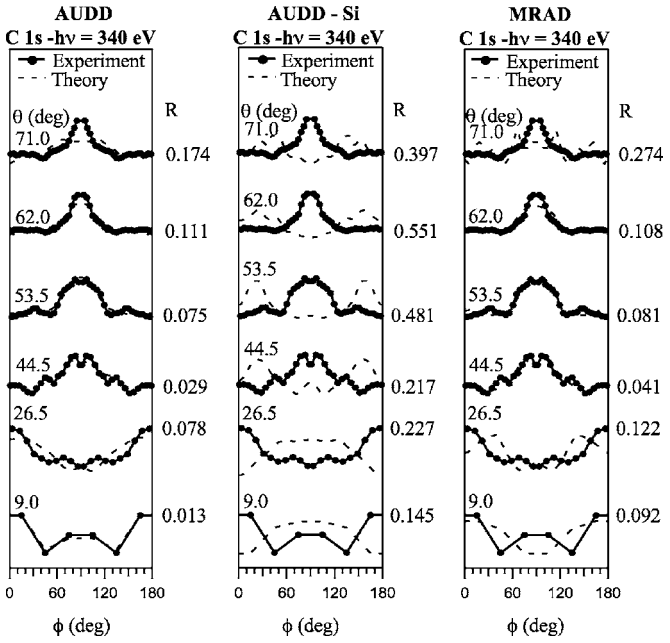

FIG. 2. Comparison between experimental (dotted lines) and theoretical anisotropy curves (dashed lines) of the C 1*s* photoemission peak as a function of azimuthal emission angle for $h\nu = 340$ eV. AUDD and MRAD models have been refined.

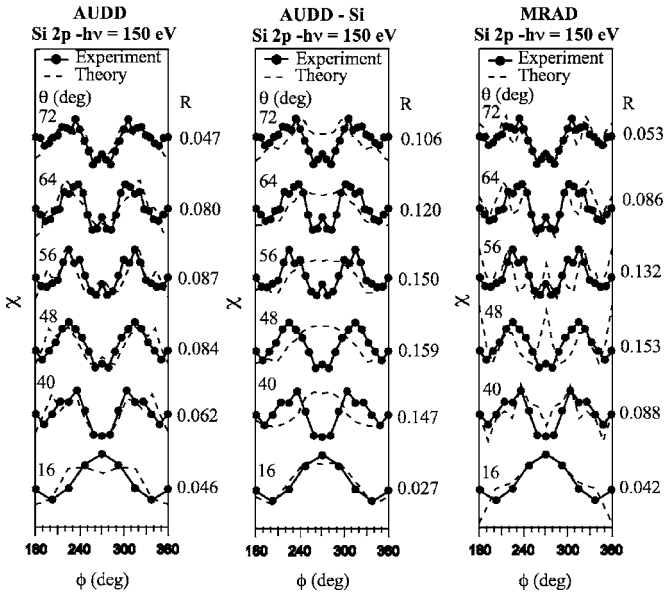

FIG. 3. Comparison between experimental (dotted lines) and theoretical anisotropy curves (dashed lines) of the Si 2*p* photoemission peak as a function of azimuthal emission angle for $h\nu = 150$ eV. AUDD and MRAD models have been refined.

relaxed such that the maximum residual force on any atom is less than 0.01 eV/Å. This is a fairly tight convergence criterion for geometry optimizations. The calculations use an energy cutoff of 400 eV for the wave functions and a spacing of the *k*-mesh of 0.3 $Å^{-1}$, which corresponds to a $3\times5\times1$ Monkhorst-Pack mesh.

IV. RESULTS

A. Atomic structure by photoelectron diffraction

A series of clusters for PED calculations reproducing the different structural models in the literature is constructed. The lattice parameter is determined as in Ref. 42. These clusters are used to model the photoelectron diffraction experimental anisotropy curves. In a first step, the theoretical simulation of the unrefined clusters is calculated and compared to the experimental curves. Although an imperfect agreement between experiment and theoretical simulation is expected for unrefined clusters, if the agreement between a model and experiment is extremely poor, the model can be safely discarded.[42] We show only MRAD, AUDD-Si, and AUDD models, since the AAD model can be obtained out of AUDD by breaking the symmetry of the dimers during the optimization of the atomic positions. Figures 2–5 show the anisotropy at different angles, different emitters, and different photon energies. The AUDD and MRAD models have both been refined, but the AUDD-Si model corresponds to an unrefined cluster.

The refinement of the MRAD and AUDD models is performed searching the best agreement with the experimental data. To this end, the surface structural parameters are systematically modified until an absolute *R*-factor minimum is found. The positions of all atoms in the topmost three layers of the cluster are changed during the structure refinement process, within a $p1m$ symmetry. The number of varied parameters is 9: six structural parameters [the height of up and down dimers, their bond lengths, and the vertical coordinates of the last C layer (C-II) and the last undimerized Si layer (Si-III)] and three nonstructural parameters (inner potential, surface position, and mean free path). The mean free path is considered also as a parameter within the order of magnitude

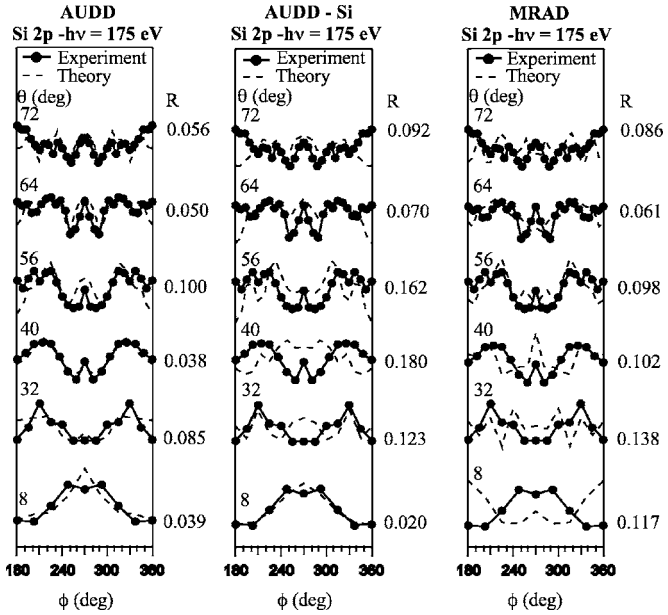

FIG. 4. Comparison between experimental (dotted lines) and theoretical anisotropy curves (dashed lines) of the Si 2*p* photoemission peak as a function of azimuthal emission angle for $h\nu = 175$ eV. AUDD and MRAD models have been refined.

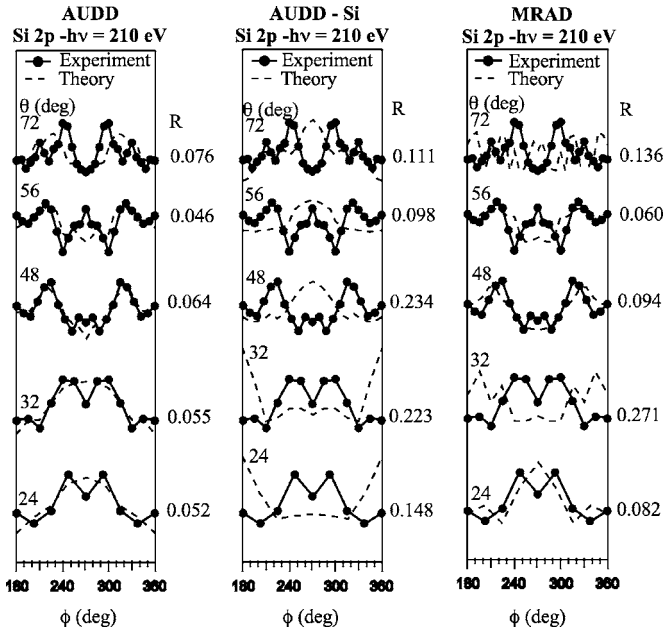

FIG. 5. Comparison between experimental (dotted lines) and theoretical anisotropy curves (dashed lines) of the Si $2p$ photoemission peak as a function of azimuthal emission angle for $h\nu$ =210 eV. AUDD and MRAD models have been refined.

defined in Ref. 59. Since the total number of experimental points is 315, there is a ratio of ~35 experimental points per parameter. In order to distinguish between AAD and AUDD models, we have explored the AAD model during the atomic refinement process of the model AUDD and/or AAD, since it is possible to switch between both models by considering inequivalent atoms within the dimers. During the refinement process of the AUDD model, atoms within each dimer are considered independent first, but the system favors a symmetric configuration. Furthermore, even when the asymmetry of one dimer is imposed, the other adopts again a symmetric disposition. The AAD model is thus discarded.

Figure 2 shows the comparison between experimental and theoretical anisotropy curves[60] for the emission of C $1s$ excited with 340 eV photons. From a visual inspection, it is clear that both AUDD and MRAD models are able to explain the experimental anisotropy curve. On the other hand, the AUDD-Si model cannot explain the experimental maxima at ϕ=90° in the azimuthal cuts between θ=44.5° and 71°. Instead of this maximum, two peaks appear more than 30° away of the experimental peak. From an R-factor analysis, it is observed that only one azimuthal cut of the MRAD model (θ=62.0°) has a lower R factor than the AUDD model (a 3% lower). The other azimuthal cuts correspond to R factors that are 8–700% worse. The difference between AUDD and AUDD-Si is even larger, since the R factor for the latter can be even 1100% of R_{AUDD}. The same analysis can be done for the Si $2p$ emission. Figures 3–5 show a representative set of the corresponding Si $2p$ experimental and theoretical anisotropies at 150, 175, and 210 eV photon energies. A visual inspection of these figures reveals that only the AUDD model is able to reproduce the general features of most of the experimental curves. In particular, if we consider $h\nu$ =150 eV and θ=48°, we observe that the MRAD model overestimates more than the AUDD model the peak at ϕ =90°. There is a similar situation at $h\nu$=175 eV and θ =40°. The photon energy of 210 eV is the most favorable for the AUDD model, although the agreement is less perfect for grazing emission angles. At this excitation energy and at θ =32°, the distribution of intensity of the MRAD model is rotated 90° with respect to the experimental pattern, while the AUDD model describes it satisfactorily. A full R-factor comparison of all individual azimuthal cuts (all energies and both emitters) favors the AUDD model, as it is reflected by the value of the mean R factor: 0.068 for AUDD, 0.180 for AUDD-Si, and 0.109 for MRAD. Therefore, the AUDD model is the only one that reproduces the overall shape of the modulation curves (as can be seen by a simple visual inspection), and in addition, it is also favored by the R-factor analysis. The results allow us to safely discard both MRAD and AUDD-Si models, which will no longer be considered in the following.

The refinement process of the AUDD model is shown in Fig. 6, where the R-factor value is represented as a function of different structural parameters. The origin of vertical coordinates is located at C-II (see Fig. 1 for the layer labeling definition). The minimum corresponds to a height difference between dimers of (0.4±0.1) Å. The bond lengths of the top and bottom dimers are (2.5±0.2) and (2.2±0.2) Å, respectively. The mean height of Si dimers over the last C layer is 0.8 Å, which is a 70% of the bulk value. Figure 1 displays a schematic of interlayer separation for the four first atomic layers Si-I, C-II, Si-III, and C-IV with distances at 0.9 Å (up dimer) and 0.6 Å (down dimer) above C-II, 1.0 Å between C-II and Si-III, and 1.1 Å between C-III and Si-IV, the latter distance corresponding to the bulk value.

B. Atomic structure by *ab initio* computations

We performed *ab initio* calculations to gain a more detailed understanding of the surface reconstruction. Of particular interest is the dependence of the reconstruction on lateral strain. An AUDD reconstruction is obtained for strains of 3%, 4%, and 5%, whereas the systems with strains between −1% and +2% converge to a flat surface with a slight tendency to dimerization of the Si atoms in the surface layer. In other words, within the present computational method, the AUDD reconstruction occurs only for systems under tensile strain. This is consistent with a previous computational study.[31] The present results are summarized in Table I. The results indicate that the AUDD reconstruction is very sensitive to the lateral distance between the Si dimers. A compression leads to a flat surface, i.e., a surface without an up-and-down reconstruction, while an expansion stabilizes the AUDD reconstruction.

At the present level of theory, i.e., density-functional theory with the generalized gradient approximation for exchange and correlation, and considering only the electronic energy as the leading term of the Gibbs free energy, an expansion of 3% is needed to cause the AUDD reconstruction to appear [Fig. 7(a)]. In the cases of +3% and +4% strains, the system converges toward a $c(4\times2)$ reconstruction. At a strain of +5%, using analogous starting conditions to those at

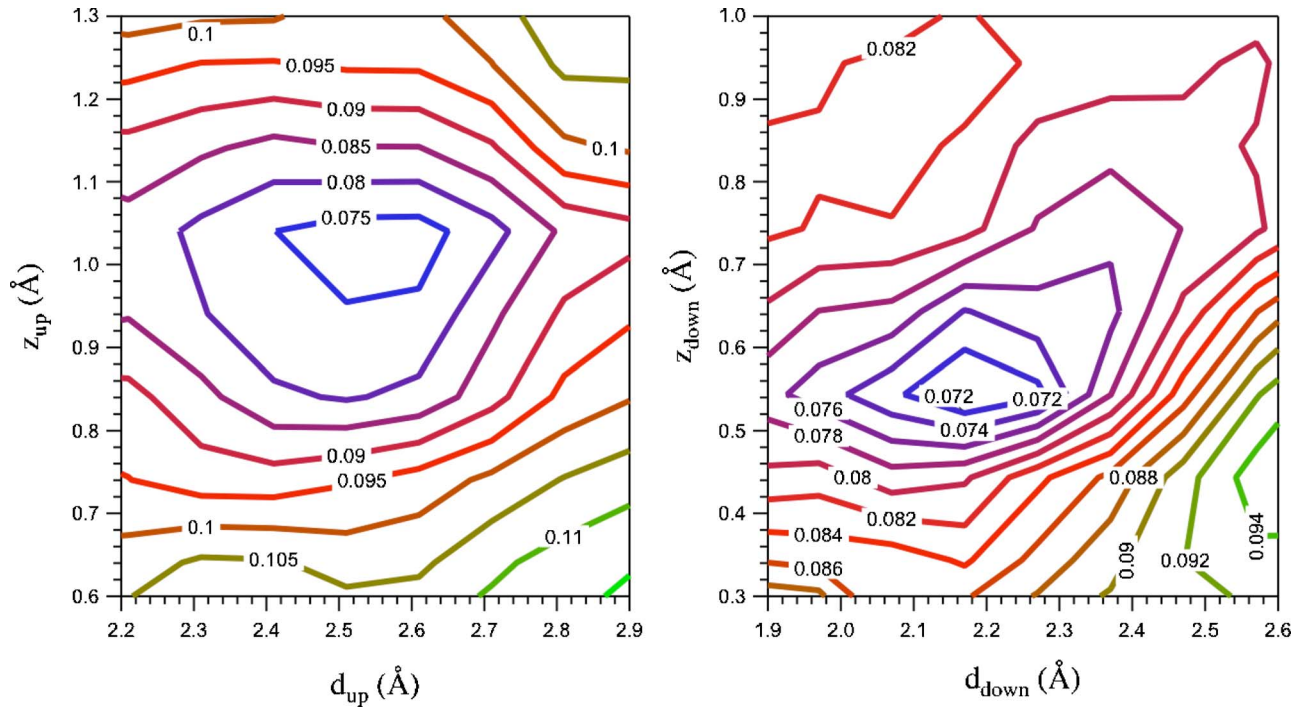

FIG. 6. (Color online) *R*-factor contour plot in the vicinity of the optimal atomic structure. z_{up} (z_{down}) are the vertical coordinates of the up (down) dimers in the last layer. d_{up} (d_{down}) are the bond lengths of the up (down) dimer. The origin of vertical coordinates ($z=0$) is located at the last layer of C atoms (see Fig. 1).

smaller strains, the system converges to a $p(2\times2)$ structure.

Further insight is gained by *ab initio* calculations of a structural model of 3*C*-SiC(001) with surface defects. The elimination of every other row without any lateral expansion of the lattice parameters leads spontaneously to the formation of AUDD structure upon full relaxation of the model [Fig. 7(b)].

The present results indicate that an increase of the spacing between Si-dimer rows favors the formation of the AUDD pattern. The spacing between dimer rows can increase either by a lateral expansion (i.e., tensile strain) or by the absence of Si dimers at the surface near steps or at vacancies. These results are perfectly consistent with earlier cluster calculations,[34] where the increase of spacing between the dimer rows is given by the finite cluster size.

TABLE I. Computed equilibrium structures of Si dimers on a reconstructed 3*C*-SiC(001) $c(4\times2)$ surface. In the case of 5% strain, the surface cell forms a $p(2\times2)$ periodicity, as explained in the text.

Strain (%)	Lateral lattice parameters (Å)		Length of dimer (Å)		Difference in height (Å)
	a	*b*	Up	Down	
−1	6.13153	12.26305	2.73	2.73	0
0	6.19346	12.38692	2.69	2.69	0
1	6.25540	12.51080	2.63	2.63	0
2	6.31733	12.63466	2.59	2.59	0
3	6.37926	12.75853	2.63	2.36	0.25
4	6.44120	12.88240	2.60	2.35	0.25
5	6.50313	13.00627	2.75	2.28	0.36

C. Identification of the Si 2*p* core-level shifted components

In the previous PED analysis, the energy-integrated experimental spectra have been employed to compare with theoretical simulations. However, the spectra also contain information about the emitters in different chemical environments. The Si 2*p* core-level deconvolution for the $c(4\times2)$ reconstruction has been established by synchrotron-radiation-based core-level photoemission spectroscopy, with two surface (S_1 and S_2) and two subsurface (SB_1 and SB_2) shifted components.[33] We have tested this deconvolution in three angular data sets, where the solid angle is varied 105 times at a constant photon energy ($h\nu=125,150,175$ eV), and three other experiments where the photon energy is varied while the solid angle is kept constant at $(\theta,\phi)=(20°,0°)$, (20°,90°), and (0°,0°), which correspond to more than 175 additional spectra. We have employed a Shirley background and five doublets of Voigt functions.[33] The branching ratio of $2p_{1/2}$ and $2p_{3/2}$ is 0.5 and the spin-orbit splitting is −0.602 eV. The Lorentzian width is 85 meV. The Gaussian width is the same for all the components of each spectrum (0.28±0.08 eV). The surface components are shifted by −1.43 eV(S_1), −0.54 eV(S_2), −0.4 eV(SB_1), and +0.31 eV(SB_2) relative to the bulk (B). The fit is obtained by a least-squares method. Figure 8 shows the deconvolution of the normal-emission spectrum at $h\nu=150$ eV.

Once the core-level deconvolution is performed, the diffraction of each component allows one to gain insight on the

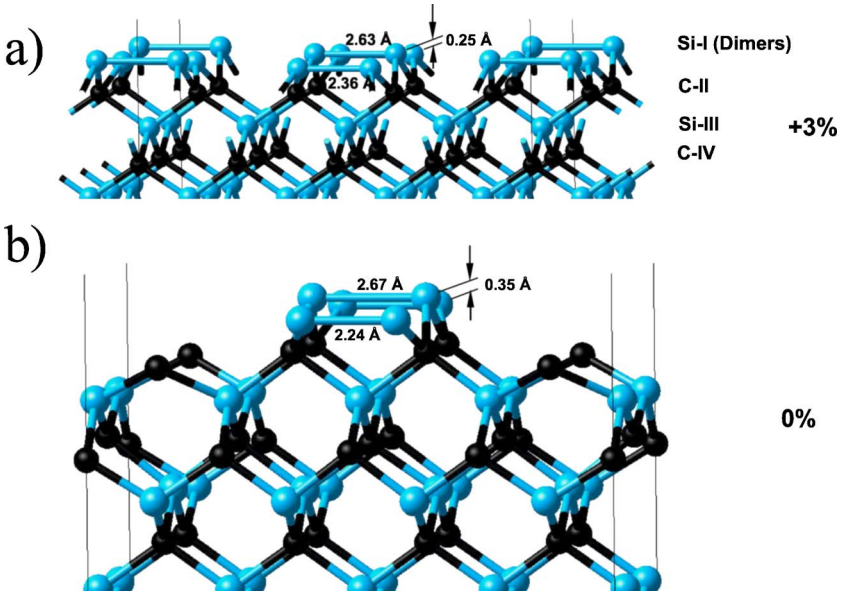

FIG. 7. (Color online) Computed (4×2) reconstruction of a SiC(001) surface. For clarity, only the top layers of the 11-layer models are shown. (a) AUDD reconstruction appears for the expanded system (+3% lateral strain). (b) AUDD structure for SiC(001) surface at 0% lateral strain with every other dimer row missing.

structure and to identify the atomic origin of the component. Figures 9 and 10 show the deconvolution for $h\nu=150$ and 210 eV along [110] and $[\bar{1}10]$ directions. The surface character of S_1 and S_2 manifests itself in an intensity increase for grazing emission for $h\nu=210$ eV. On the other hand, the higher surface sensitivity of $h\nu=150$ eV allows us to observe S_1 in the whole polar angular range shown.

A detailed understanding on the physical origin of the different components can be gained from an analysis of their intensities. Figure 11(a) shows the intensities along the polar cut at $\phi=0°$ for $h\nu=150$ eV. It is observed that B decreases at grazing emission, as it corresponds to the bulk component. SB_1 exhibits a similar behavior, but its intensity at grazing emission is higher, which suggests a partial surface character. SB_2 presents maxima and minima at the same angles as SB_1 and B, which indicates a similar origin. S_1 and S_2 have a surface origin, as their intensities are enhanced at grazing emission. Figure 11(b) shows the evolution of the components for a constant initial state experiment, where normal-emission electrons are detected while the photon energy is varied between 147 and 332 eV. The figure shows that B, SB_1, and SB_2 present correlated oscillations, whereas S_1 and S_2 are uncorrelated to the previous components.

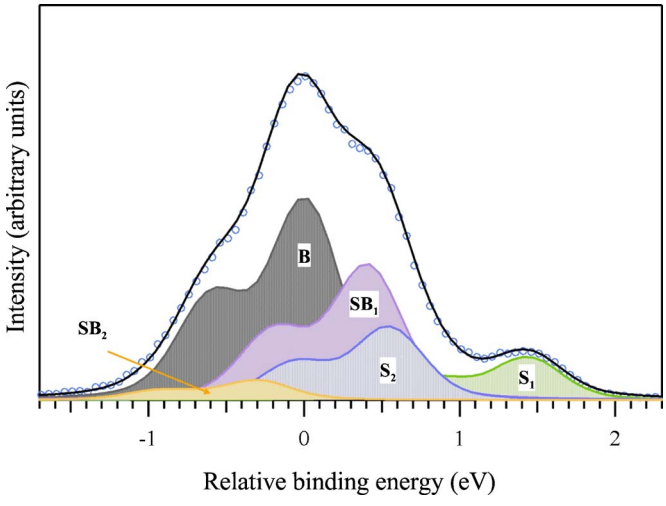

FIG. 8. (Color online) Normal-emission Si $2p$ core level at $h\nu=150$ eV. The experimental spectrum is represented by circles and the fit with a continuous line. The different components are also shown (see text for more details). The binding energy is referred to the $2p_{3/2}$ peak of the bulk component.

The weight of one kind of emitter is related to the intensity of the associated component. Although this type of analysis can be affected by the diffraction effects, which can be rather strong, these effects can be overcome by considering a large number of spectra as a function of photon energy, solid angle, or both. Figure 11(b) shows similar intensities for S_1 and S_2 and a higher SB_1 intensity. Therefore, the populations P are qualitatively $P(SB_1)>P(S_1)\sim P(S_2)$. All these results support the previous Si $2p$ core-level photoemission study[33] and settle the starting point for a more detailed and in-depth identification of the surface and/or subsurface shifted components by photoelectron diffraction.

The identification of the surface atomic environment by photoelectron diffraction relies on the comparison between the simulated PED pattern for a given emitter type and the experimental pattern for a single component. In the $c(4\times2)$ reconstruction, there are three different surface environments for the Si atoms: the top dimers, the bottom dimers, and the first undimerized Si layer (Si-III), located below the first C plane (C-II) with a distance between them smaller than the bulk separation. S_1 and S_2 could be associated with the two different types of dimers (up and down) of 3C-SiC(001)-$c(4\times2)$. The different core-level shift would reflect a charge transfer between up and down dimers, similar to the one observed in the asymmetric dimers of Si(001)-$c(4\times2)$ between the up and down atoms. The last undimerized Si layer (Si-III) would be associated with SB_1, with a larger number of emitters than S_1 or S_2. Figure 12 shows the experimental azimuthal cuts obtained for the different components of the deconvolution of Si $2p$ and the comparison with simulated azimuthal cuts from a given Si environment. Since S_1 and S_2 present the largest chemical

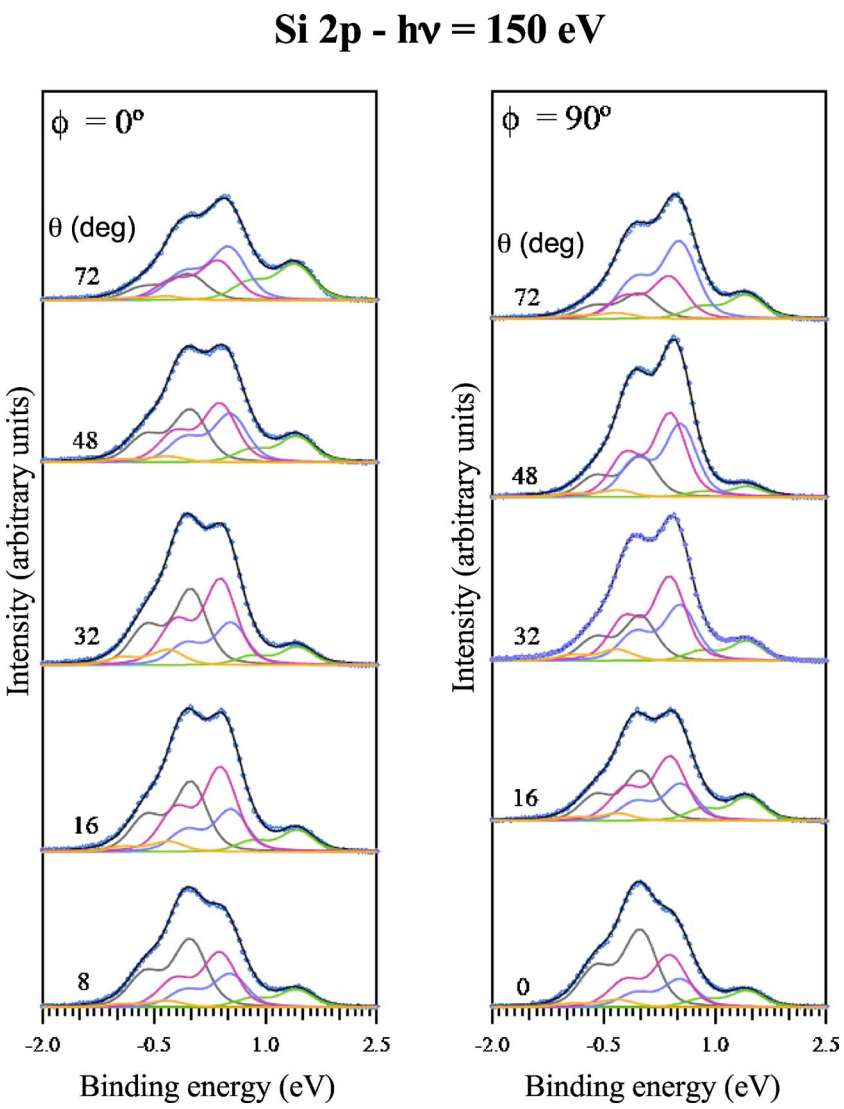

FIG. 9. (Color online) Si $2p$ deconvolution along the directions [110] (ϕ=0°) and [−110] (ϕ =90°). The core level is shown as a function of polar angle θ for $h\nu$=150 eV.

shifts, they should correspond to the most surface sensitive components. These components have been compared with the simulated emission of the top dimers, the bottom dimers, or all the dimers together. The experimental maxima of S_2 at ϕ=0° cannot be reproduced with the emission of the top dimers. In consequence, S_2 cannot correspond to the top dimers. Furthermore, the superposition of the simulated PED signal of the whole layer of dimers (not shown) originates a significant diffraction maximum at ϕ=0°, which prevents the assignment of the whole last layer to S_1. We conclude that the only possible assignment is the one shown in Fig. 12, which attributes S_1 to up dimers and S_2 to down dimers. The assignment of the theoretical emission of Si-III to SB_1 corresponds to an R factor 30–50% more favorable than the comparison with SB_2 or B. SB_1 must therefore correspond to Si-III, i.e., the last undimerized Si layer. The R factors associated with the comparison of the theoretical emission of Si-IV with the experimental azimuthal cuts of SB_2 or B differ only by 4%. These components have therefore a similar origin, as already suggested from their similar and large photoelectron escape depth.[33] Their similar nature has led us to consider just one theoretical component associated with the emitters at Si-IV and deeper. We have compared this theoretical component with the experimental azimuthal cut of B. The theoretical azimuthal cuts within this assignment are shown in Fig. 12. The excellent agreement between photoelectron diffraction simulations and experimental data for each surface component allows us to understand unambiguously their origin.

Once the identification of the components is finished, it is also possible to check the consistency of the model by deriving the model structure from the PED analysis of a single surface component. Figure 13 shows the diffraction anisotropy of S_1 along a constant direction (20° off normal along the [110] direction) as a function of photon energy. The selected photon energies correspond to the low kinetic energy regime, which is particularly difficult to simulate due to multiple-scattering effects, as it happens also in LEED. A variation of the structural parameters affects the interference pattern, which is produced by the backscattering of Si $2p$ photoelectrons emitted by the top dimers. The value of the R factor has been minimized by changing the structural parameters of the reconstruction. The minimum is reached for the simulation shown in Fig. 12, which corresponds to a height difference Δz=(0.4±0.1) Å and a top dimer bond length =(2.5±0.2) Å. Therefore, we recover the same parameters of

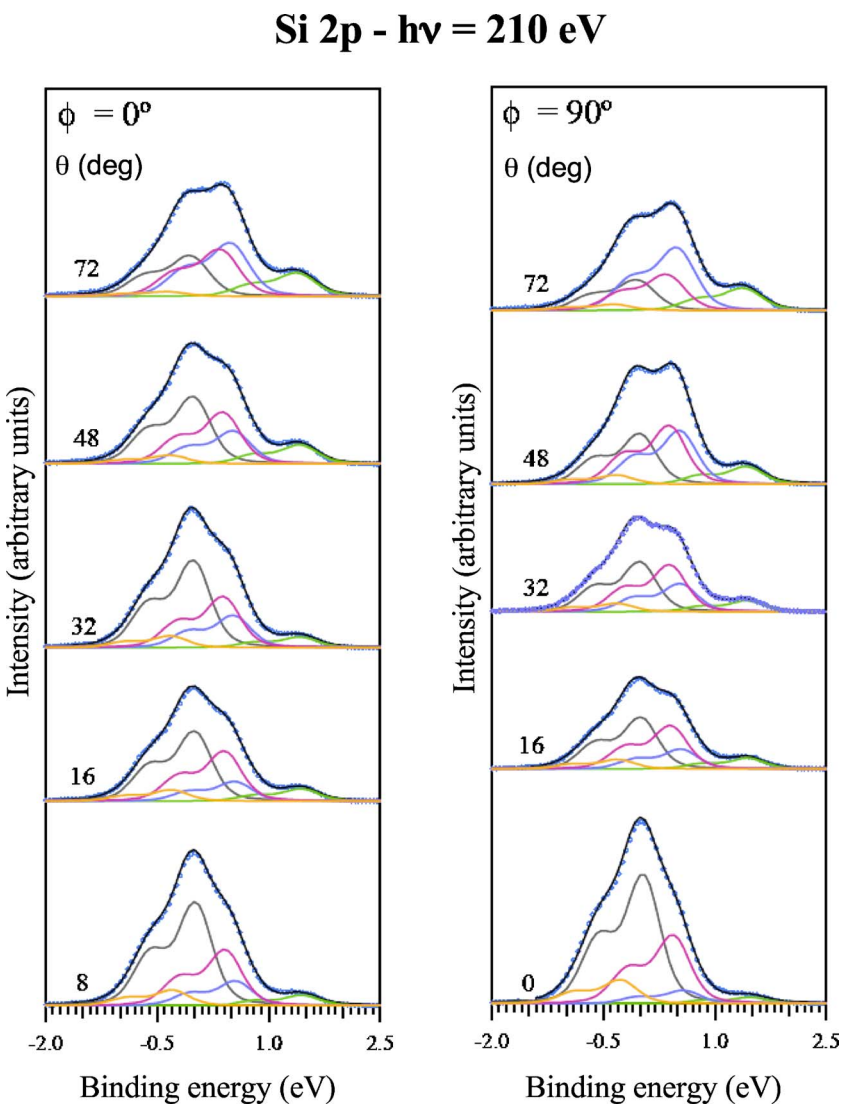

FIG. 10. (Color online) Si $2p$ deconvolution along the directions [110] (ϕ=0°) and [−110] (ϕ=90°). The core level is shown as a function of polar angle θ for $h\nu$=210 eV.

the integrated spectrum analysis in an independent way, which further supports the AUDD structural model of the $c(4\times2)$ reconstruction, together with the assignment of the surface and subsurface components.

V. DISCUSSION

Our present combined photoelectron diffraction experiments and *ab initio* total-energy calculations determine the complete atomic structure of the $c(4\times2)$ reconstruction, providing a strong evidence that the 3*C*-SiC(001) $c(4\times2)$ surface is organized in an AUDD array. This model of the reconstruction has been initially proposed on the basis of STM measurements and later supported by *ab initio* total-energy calculations, and experimental investigations on the core levels and the electronic properties of the surface.[26,29–34] Consistent with previous experimental results (STM, MEIS, core-level PES, and valence-band PES)[24,26,29,30,32,33] and earlier *ab initio* total-energy calculations,[31,34] the present comprehensive structural investigation based on PED and combined with *ab initio* calculations is clearly inconsistent with the MRAD model, predicted by *ab initio* pseudopotential calculations.[35,36] The $c(4\times2)$ surface is terminated by a Si atomic layer (1 ML) on top of the first C plane. Also of special interest are the alternating lengths of the top-surface Si dimers found to be (2.5±0.2) and (2.2±0.2) Å with a height difference of (0.4±0.1) Å, in excellent agreement with the present *ab initio* calculations for surface strains of 3% (2.63 Å and 2.36 Å) and 4% (2.60 Å and 2.35 Å), both with a height difference of 0.25 Å (see Table II). Also, model calculations with surface defects (missing Si-dimer rows) at 0% lateral strain show alternating bond lengths of 2.67 and 2.24 Å with a height difference of 0.35 Å [Fig. 7(b)]. The remarkable agreement between calculations and the PED experimental results clearly supports strain relief to be at the origin of this very special surface reconstruction.

This interesting aspect deserves further discussion. Previous calculations, as well as those presented here, found that the $c(4\times2)$ reconstruction exists only when a strain is applied to the semi-infinite model used for computing, which otherwise would give a (2×1) structure with dimers all having the same lengths and heights.[31] The source of this remarkable behavior of the 3*C*-SiC(001) surface is the large lattice mismatch difference between SiC and Si (−20%) or C

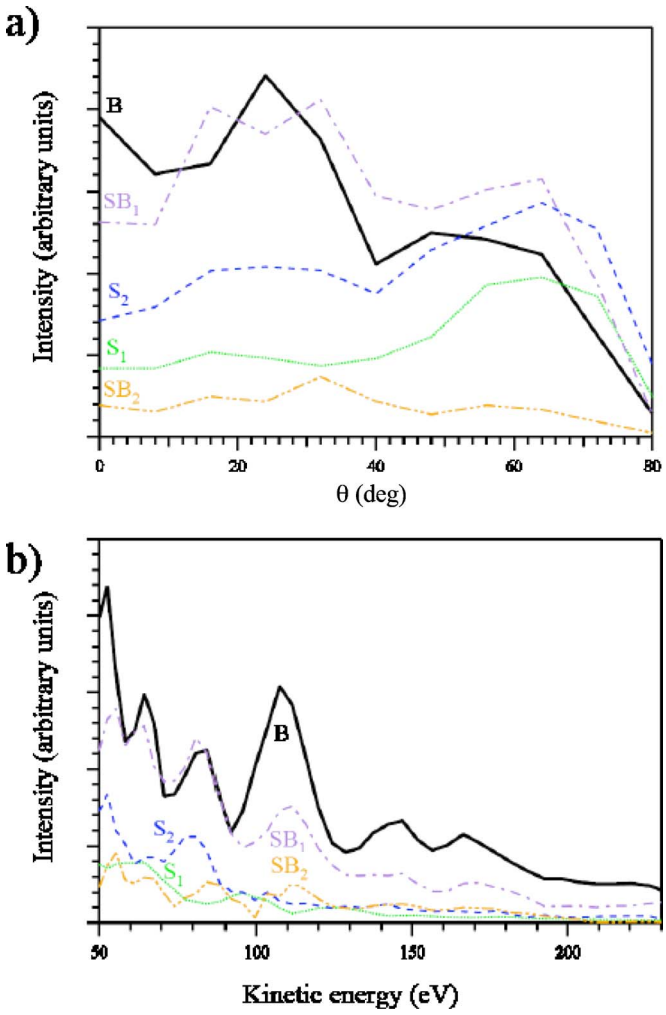

FIG. 11. (Color online) Amplitude of the different components of the Si $2p$ core level. (a) Polar cut at $\phi=0°$ and $h\nu=150$ eV. (b) Constant initial state experiment at normal emission.

(+22%).[26] The very peculiar character of the AUDD surface array for the $3C$-SiC(001) $c(4\times2)$ surface, with rows of alternating up and down and long and short dimers, supports the picture of strain as the leading driving force in surface organization. The present results are also of interest in view of the temperature-induced reversible $c(4\times2)$ to (2×1) metallic phase transition.[29] The calculations reveal a very small difference in the electronic energy between the AUDD $c(4\times2)$ and the flat (2×1) phases of the SiC(001) surface. The stability of a phase as a function of temperature is determined by the Gibbs free energy, $\Delta G=\Delta H-T\Delta S$. The small energy difference between the AUDD and the flat surface structures indicates a low vibrational frequency for vertical motions of dimers and a small energy barrier for flipping the height of up and down dimers. Both facts lead to a large vibrational entropy. Thus, it is reasonable to expect that at elevated temperatures, the system escapes from the shallow local minima of the AUDD structure and transforms into a flat surface with an effective (2×1) structure, which is stabilized by the vibrational entropy term $-T\Delta S$.

Another very interesting feature of the above photoelectron diffraction results is the confirmation of the Si $2p$ core-level curve fitting deconvolution into two surface (S_1 and S_2) and two subsurface (SB_1 and SB_2) shifted components (Fig. 8).[33] It strongly supports the assignment of the S_1 and S_2 surface shifted components to the up dimer and down dimer, respectively.[33] The large binding-energy difference relative to the bulk component (−1.43 eV for S_1 and −0.54 eV for S_2) indicates a different electronic character between both dimers (Fig. 8), also in agreement with previous results.[33] As indicated above, this further explains why the up dimer is seen almost "filled" in STM topographs, while the down dimer is partially filled and partially empty, making possible STM imaging at both filled and empty states.[26,30] Also, the height difference between the up and the down dimers measured by PED is (0.4±0.1) Å. This value compares well with measurements performed by STM, which give height differences of 0.2–0.25 Å, keeping in mind that STM measures electronic distances rather than geometric ones.

Most interestingly, the photoelectron diffraction experiment allows us to assign the two subsurface shifted components SB_1 and SB_2, initially identified by Si $2p$ core-level photoemission spectroscopy.[33] SB_1 is due to the contribution of the third atomic layer [Si-III in Fig. 1(b)]. On the other hand, SB_2, which is located at 0.31 eV higher binding energy relative to the bulk B component, seems to have predominantly a bulk character, since the corresponding photoelectron diffraction pattern is similar to the one of the bulk B component. Such a behavior is in excellent agreement with previous core-level photoemission spectroscopy probing the photoelectron escape depth at SB_2.[33] This interesting aspect clearly indicates that the Si atoms located below the surface (deeper than the Si-III atomic layer) are not fully in bulk positions and/or have a charge transfer toward C atoms still larger than that of "bulk" Si atoms, as stressed by a higher binding energy (by 0.31 eV) compared to the bulk B component. It is also interesting to remark that without a strain of at least 3%, all the dimers have not only the same height but also the same length (2.69 Å) at 0% strain, i.e., a value well above the average lengths of both short and long dimers at 3% (2.63 and 2.36 Å) or more strain (Table I). Such a situation is likely to result in efficient and uneven charge transfer toward the $c(4\times2)$ surface and subsurface compared to a hypothetical (2×1) surface, as indeed shown above by the shifted components at the Si $2p$ core level.

Another aspect is provided by the *ab initio* calculations of slab models, showing a very subtle energy difference between a flat (2×1) reconstruction and a $c(4\times2)$ AUDD reconstruction. Minimization of the electronic energy leads to an AUDD structure, provided that a lateral tensile strain greater than 3% is applied, for instance, if vacancies in the form of missing Si-dimer rows are introduced. Otherwise, a flat (2×1) structure is obtained. The computed structural parameters for the AUDD surface are in excellent agreement with the present experimental results. For a lattice with a 3% lateral expansion, the corrugation is 0.25 Å and the bond distances in the up and down dimers are 2.63 and 2.36 Å, respectively. For the case of no lateral strain, but with defects in the form of missing Si-dimer rows, the corresponding values are 0.35, 2.67, and 2.24 Å. These values are within the experimental errors bars given above. Taken together, these

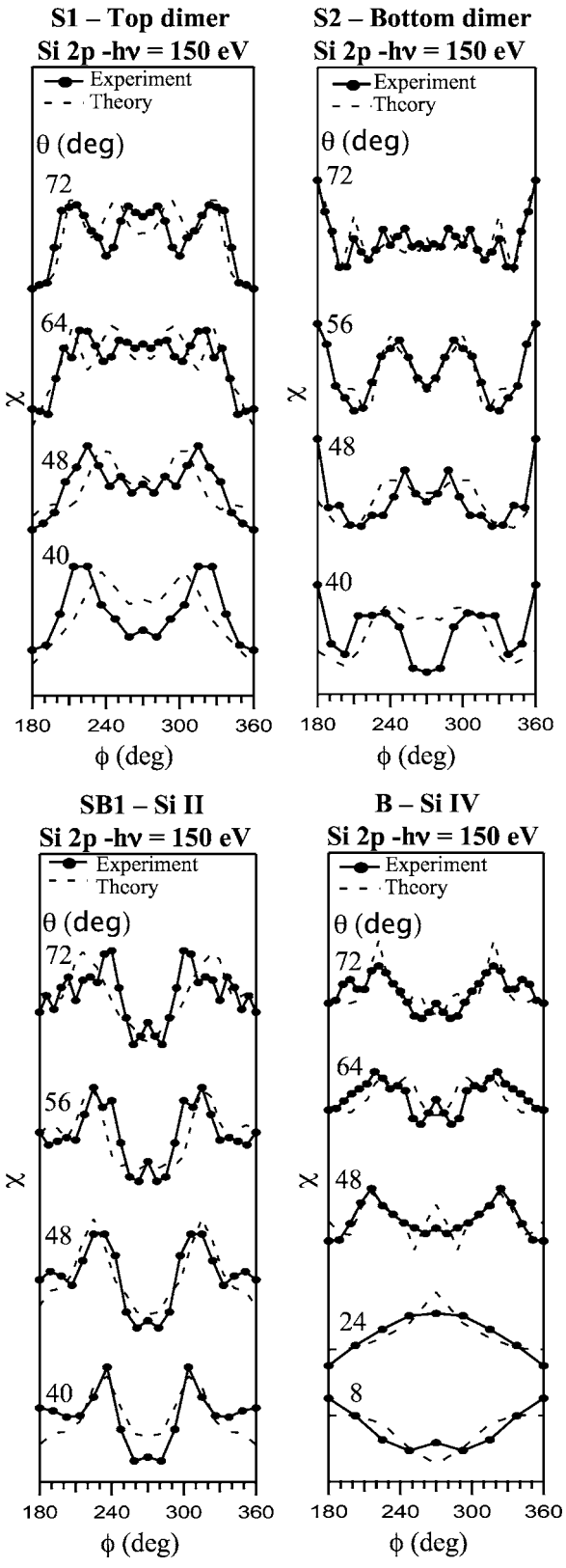

FIG. 12. Experimental intensities of the components of Si 2*p* core level along different azimuthal cuts. S_1 is compared with the simulated emission of the top dimer, S_2 with the simulated emission of the bottom dimer, SB_1 with the simulated emission of Si-III layer, and B with the simulated emission from the remaining layers.

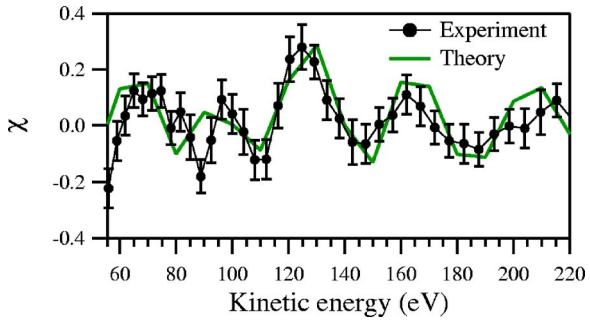

FIG. 13. (Color online) Comparison of experimental Si 2*p* S interference pattern with the results of multiple-scattering calculations for the top dimers in the best-fit structure (20° off normal along the [110] direction).

results provide additional strong evidence for the existence of an AUDD reconstruction.

The dependence of the AUDD reconstruction on the lateral strain is remarkable. Intuitively, one might expect that a compression leads to a corrugation and an expansion (tensile strain) would cause a flattening of the surface. The calculations give the opposite trend. This result shows that (i) the response of the surface electronic structure to lateral strain is important and nontrivial and (ii) effects due to the vibrational entropy associated with the thermal motion of the Si surface dimers play a role in the temperature-induced surface phase transition from the $c(4\times2)$ to the (2×1) structure.

It is unlikely that differences in the Hamiltonian and the computational methodology used in the present work compared with that underlying the prediction of the MRAD model are significant. Most likely, the MRAD structure is indeed a local minimum on the energy hypersurface of the Si-C system, but it is not the structure that is formed under the present experimental conditions.

The $c(4\times2)$ reconstruction of the 3*C*-SiC(001) surface is therefore explained by two different analyses of PED experiments and by *ab initio* computations. This reconstruction appears to be very different from the corresponding $c(4\times2)$ reconstruction of the Si(001) or Ge(001) surfaces, which appear under Jahn-Teller distortions tilting the dimers in opposite senses along the rows. In this case, the anticorrelation of the tilt between dimers in adjacent rows is at the origin of the $c(4\times2)$ symmetry for the Si(001) surface.[61] For 3*C*-SiC(001), the situation is completely different with alternating up (long) and down (short) symmetric dimers along the row.

VI. CONCLUSIONS

We report a detailed crystallographic investigation of the 3*C*-SiC(001)-$c(4\times2)$ surface reconstruction using synchrotron-radiation-based photoelectron diffraction and *ab initio* total-energy and generalized gradient approximation theoretical calculations. Both experimental and theoretical results support that the $c(4\times2)$ reconstruction is described by the AUDD model, but are not consistent with a MRAD picture. Strain is the driving force in the $c(4\times2)$ surface organiza-

TABLE II. Up (d_U) and down (d_D) dimer bond lengths and height difference (Δz) from this work (theoretical and experimental) and from previous (theoretical) studies. The calculations of Catellani *et al.* in Ref. 31 and of this work consider a 3% strain.

Parameter	Theoretical (Ref. 34)	Theoretical (Ref. 37)	Theoretical (This work)	STM (Refs. 29 and 33)	PED (This work)
d_U (Å)	2.59	2.50	2.63		2.5±0.2
d_D (Å)	2.53	2.27	2.36		2.2±0.2
Δz (Å)	0.06	0.23	0.25	0.2–0.25	0.4±0.1

tion, leading to dimer rows having not only alternating heights (AUDD) but also alternating lengths, the up dimer being longer (2.5±0.2 Å) than the down dimer (2.2±0.2 Å), with a height difference of (0.4±0.1) Å as determined by PED. These experimental values are in excellent agreement with the distance obtained by the *ab initio* VASP calculations at 2.63, 2.36, and 0.25 Å, respectively, for a 3% lateral strain. A conclusive identification of the origin of the surface shifted components is made from a comparison of their experimental photoelectron diffraction with the different atomic environments of the AUDD model. Two surface components are related to the up and down dimers and two other components are related with the subsurface atomic layers. It also supports up and down dimers having different electronic characters, in agreement with high-resolution filled and empty state STM topographs. This study demonstrates the importance of strain and surface defects in SiC surface organization. Thus, a more detailed understanding of one of the remarkable surface reconstructions of SiC has been gained. It is hoped that this will form a solid basis for future work on this promising material, opening up further investigations such as the interaction of metallic or molecular adsorbates and the self-organization of nano-objects.

ACKNOWLEDGMENTS

The authors are especially grateful to the Advanced Light Source (LBNL, Berkeley) staff for expert and outstanding assistance. The authors thank L. di Ciccio and C. Jaussaud (CEA-LETI, Grenoble) for high quality SiC thin films and F. García de Abajo for providing the multiple-scattering code and for helpful discussions. This work was supported in part by MEC and CAM (Spain) (FIS2005-00747 and S-0505/PPQ/0316). The synchrotron radiation experiments were supported by the U.S. National Science Foundation (NSF) through the Northern Illinois University and by the Northern Illinois University Graduate School Funds.

*Also at: Laboratoire Matériaux et Phénomènes Quantiques, Université Denis Diderot Paris 7, UMR-CNRS 7162, case 7021, 2 place Jussieu, 75251 Paris, France.

[1] *Silicon Carbide and Related Materials 2005*, edited by Robert P. Devaty, David J. Larkin, and Stephen E. Saddow [Mater. Sci. Forum **527-529** (2006)].
[2] *Silicon Carbide Electronic Devices and Materials*, special issue of MRS Bull. **22** (1997).
[3] *Silicon Carbide Electronic Devices*, special issue of IEEE Trans. Electron Devices **46** (1999), and references therein.
[4] V. M. Aroutiounian, V. V. Bouniatian, and P. Soukiassian, Solid-State Electron. **43**, 343 (1999).
[5] *Silicon Carbide; A Review of Fundamental Questions and Applications to Current Device Technology*, edited by W. J. Choyke, H. M. Matsunami, and G. Pensl (Akademie Verlag, Berlin, 1998), Vols. I and II, and references therein.
[6] M. Stutzmann, J. A. Garrido, M. Eickhoff, and M. S. Brandt, Phys. Status Solidi A **203**, 3424 (2006).
[7] P. Soukiassian, F. Semond, A. Mayne, and G. Dujardin, Phys. Rev. Lett. **79**, 2498 (1997).
[8] L. Douillard, V. Yu. Aristov, F. Semond, and P. Soukiassian, Surf. Sci. Lett. **401**, L395 (1998).
[9] V. Yu. Aristov, L. Douillard, and P. Soukiassian, Surf. Sci. Lett. **440**, L825 (1999).
[10] V. Derycke, P. Fonteneau, Y. K. Hwu, and P. Soukiassian, Appl. Phys. Lett. **88**, 022105 (2006).
[11] P. Deak, A. Buruzs, A. Gali, and Th. Frauenheim, Phys. Rev. Lett. **96**, 236803 (2006).
[12] V. Derycke, P. Soukiassian, F. Amy, Y. J. Chabal, M. D'angelo, H. Enriquez, and M. Silly, Nat. Mater. **2**, 253 (2003).
[13] M. G. Silly, C. Radtke, H. Enriquez, P. Soukiassian, S. Gardonio, P. Moras, and P. Perfetti, Appl. Phys. Lett. **85**, 4893 (2004).
[14] J. Roy, V. Yu. Aristov, C. Radtke, P. Jaffrennou, H. Enriquez, P. Soukiassian, P. Moras, C. Spezzani, C. Crotti, and P. Perfetti, Appl. Phys. Lett. **89**, 042114 (2006).
[15] F. Amy and Y. Chabal, J. Chem. Phys. **119**, 6201 (2003).
[16] V. Derycke, P. Fonteneau, N. P. Pham, and P. Soukiassian, Phys. Rev. B **63**, 201305(R) (2001).
[17] P. Soukiassian and H. Enriquez, J. Phys.: Condens. Matter **16**, S1611 (2004), and references therein.
[18] V. M. Bermudez, Phys. Status Solidi B **202**, 447 (1997), and references therein.
[19] S. Mizuno, T. Shirasawa, Y. Shiraishi, and H. Tochihara, Phys. Rev. B **69**, 241306 (2004).
[20] F. Bechstedt, A. A. Stekolnikov, J. Furthmüller, and P. Käckell, Phys. Rev. Lett. **87**, 016103 (2001).
[21] K. Seino, W. G. Schmidt, and F. Bechstedt, Phys. Rev. Lett. **93**, 036101 (2004).
[22] S. Ferrer, X. Torrelles, V. H. Etgens, H. A. van der Vegt, and P. Fajardo, Phys. Rev. Lett. **75**, 1771 (1995).

[23] R. Kaplan, Surf. Sci. **215**, 111 (1989); J. Vac. Sci. Technol. A **6**, 829 (1989).
[24] S. Hara, W. F. J. Slijkerman, J. F. van der Veen, I. Ohdomari, S. Misawa, E. Sakuma, and S. Yoshida, Surf. Sci. Lett. **231**, L196 (1990).
[25] M. L. Shek, Surf. Sci. **349**, 317 (1996).
[26] P. Soukiassian, F. Semond, L. Douillard, A. Mayne, G. Dujardin, L. Pizzagalli, and C. Joachim, Phys. Rev. Lett. **78**, 907 (1997).
[27] L. Douillard, O. Fauchoux, V. Aristov, and P. Soukiassian, Appl. Surf. Sci. **166**, 220 (2000).
[28] A. Catellani, G. Galli, and F. Gygi, Phys. Rev. Lett. **77**, 5090 (1996).
[29] V. Yu. Aristov, L. Douillard, O. Fauchoux, and P. Soukiassian, Phys. Rev. Lett. **79**, 3700 (1997).
[30] V. Derycke, P. Fonteneau, and P. Soukiassian, Phys. Rev. B **62**, 12660 (2000).
[31] A. Catellani, G. Galli, F. Gygi, and F. Pellacini, Phys. Rev. B **57**, 12255 (1998).
[32] V. Yu. Aristov, P. Soukiassian, A. Catellani, R. Di Felice, and G. Galli, Phys. Rev. B **69**, 245326 (2004).
[33] V. Yu. Aristov, H. Enriquez, V. Derycke, P. Soukiassian, G. Le Lay, C. Grupp, and A. Taleb-Ibrahimi, Phys. Rev. B **60**, 16553 (1999).
[34] L. Douillard, F. Semond, V. Yu. Aristov, P. Soukiassian, B. Delley, A. Mayne, G. Dujardin, and E. Wimmer, Mater. Sci. Forum **264-268**, 379 (1998).
[35] W. Lu, P. Krüger, and J. Pollmann, Phys. Rev. Lett. **81**, 2292 (1998).
[36] S. A. Shevlin and A. J. Fisher, Phys. Rev. B **62**, 6904 (2000).
[37] G. Binnig, H. Rohrer, Ch. Gerber, and E. Weibel, Phys. Rev. Lett. **50**, 120 (1983).
[38] K. Takayanagi, Y. Tanishiro, M. Takahashi, and S. Takahashi, J. Vac. Sci. Technol. A **3**, 1502 (1985).
[39] F. Semond, P. Soukiassian, A. Mayne, G. Dujardin, L. Douillard, and C. Jaussaud, Phys. Rev. Lett. **77**, 2013 (1996).
[40] J. Powers, A. Wander, M. A. van Hove, and G. A. Somorjai, Surf. Sci. **260**, L7 (1992).
[41] M. D'angelo, H. Enriquez, V. Yu. Aristov, P. Soukiassian, G. Renaud, A. Barbier, M. Noblet, S. Chiang, and F. Semond, Phys. Rev. B **68**, 165321 (2003).
[42] A. Tejeda, D. Dunham, F. J. García de Abajo, J. D. Denlinger, E. Rotenberg, E. G. Michel, and P. Soukiassian, Phys. Rev. B **70**, 045317 (2004).
[43] J. M. Powers, A. Wander, P. J. Rous, M. A. Van Hove, and G. A. Somorjai, Phys. Rev. B **44**, 11159 (1991).
[44] J. P. Long, V. M. Bermudez, and D. E. Ramaker, Phys. Rev. Lett. **76**, 991 (1996).
[45] H. W. Yeom, M. Shimomura, J. Kitamura, S. Hara, K. Tono, I. Matsuda, B. S. Mun, W. A. R. Huff, S. Kono, T. Ohta, S. Yoshida, H. Okuski, K. Kajimura, and C. S. Fadley, Phys. Rev. Lett. **83**, 1640 (1999).
[46] C. S. Fadley, M. A. Van Hove, Z. Hussain, A. P. Kaduwela, R. E. Couch, Y. J. Kim, P. M. Len, J. Palomares, S. Ryce, S. Ruebush, E. D. Tober, Z. Wang, R. X. Ynzunza, H. Daimon, H. Galloway, M. B. Salmeron, and W. Schattke, Surf. Rev. Lett. **4**, 421 (1997).
[47] A. Tejeda and E. G. Michel, J. Phys.: Condens. Matter **16**, S3441 (2004), and references therein.
[48] M. C. Asensio, E. G. Michel, J. Alvarez, C. Ocal, R. Miranda, and S. Ferrer, Surf. Sci. **211/212**, 31 (1989).
[49] A. Mascaraque, J. Avila, C. Teodorescu, M. C. Asensio, and E. G. Michel, Phys. Rev. B **55**, R7315 (1997).
[50] Y. Chen and M. A. Van Hove, http://electron.lbl.gov/mscdpack/; F. J. Garcia de Abajo, M. A. Van Hove, and C. S. Fadley, Phys. Rev. B **63**, 075404 (2001).
[51] S. Tanuma, C. J. Powell, and D. R. Penn, Surf. Interface Anal. **21**, 165 (1993).
[52] R. S. Saiki, A. P. Kaduwela, M. Sagurton, J. Osterwalder, D. J. Friedman, C. S. Fadley, and C. R. Brundle, Surf. Sci. **282**, 33 (1993).
[53] M. A. Van Hove, S. Y. Tong, and M. H. Elconin, Surf. Sci. **64**, 85 (1977).
[54] P. Hohenberg and W. Kohn, Phys. Rev. **136**, B864 (1964); W. Kohn and L. J. Sham, Phys. Rev. **140**, A1133 (1965).
[55] J. P. Perdew, K. Burke, and M. Ernzerhof, Phys. Rev. Lett. **77**, 3865 (1996).
[56] P. E. Blöchl, Phys. Rev. B **50**, 17953 (1994).
[57] G. Kresse and J. Hafner, Phys. Rev. B **47**, 558 (1993); G. Kresse and J. Furthmüller, *ibid.* **54**, 11169 (1996); Comput. Mater. Sci. **6**, 15 (1996); G. Kresse and D. Joubert, Phys. Rev. B **59**, 1758 (1999).
[58] MEDEA 2.0, Materials Design, Inc., Taos, NM, 2005 (www.materialsdesign.com).
[59] S. Tanuma, C. J. Powell, and D. R. Penn, Surf. Interface Anal. **17**, 927 (1991).
[60] D. P. Woodruff and A. M. Bradshaw, Rep. Prog. Phys. **57**, 1029 (1994).
[61] R. A. Wolkow, Phys. Rev. Lett. **68**, 2636 (1992).